# The scattering cross sections for $^{6,7}$Li + *n* reactions

D.Ichinkhorloo [1], M. Aikawa [1], S. Chiba [2], Y.Hirabayashi [3], and K. Katō [1]

[1]*Nuclear Reaction Data Centre, Faculty of Science, Hokkaido University, Sapporo 060-0810, Japan*
[2]*Research Laboratory for Nuclear Reactors, Tokyo Institute of Technology, Tokyo 152-8550, Japan*
[3]*Information Initiative Center, Hokkaido University, Sapporo 060-0811, Japan*

**Abstract.** We investigate the continuum-discretized coupled-channel analysis to the integrated elastic and inelastic scattering cross sections for $^{6,7}$Li + *n* reactions. We used the Jeukenne-Lejeune-Mahaux effective nucleon-nucleon interaction and optical model potential at incident neutron energies below and above 10 MeV, respectively. The calculated elastic and inelastic scattering cross sections with observed incident energies are almost in good agreement with experimental and evaluated data.

## 1 Introduction

The Li + *n* reactions are important not only from the basic interest but also from the application point of view. Lithium isotopes will be used as a tritium-breeding material in the *d-t* fusion reactors. Therefore accurate nuclear data are required for n- and p-induced reactions.

In the previous works [1-3], we have successfully studied cross sections for the $^{6,7}$Li + *n* elastic and inelastic scattering angular distributions and neutron spectra applying the continuum-discretized coupled-channel method (CDCC) method [4] with ($\alpha$ - *d*) + *n* and ($\alpha$ - *t*) + *n* models. It was found that the observed cross section data for incident energies from 7.47 to 24 MeV can be reproduced by the present cluster model with one normalization parameter for the imaginary part of the Jeukenne-Lejeune-Mahaux effective nucleon-nucleon (JLM) [5] interaction. More recently, H. Guo et al. [6] have analyzed both neutron and proton scatterings from $^{6,7}$Li in wide incident energies up to 150 MeV, and demonstrated the applicability of CDCC to nucleon scatterings from $^{6,7}$Li. They analyzed neutron total cross sections, proton reaction cross sections and differential cross sections for nucleon elastic and inelastic scatterings. However, it is still difficult to reproduce low energy data below 14.1 MeV in these frameworks.

In this work, we extended the CDCC analysis to the integrated elastic and inelastic scattering cross sections for $^{6,7}$Li at incident neutron energies below 10 MeV by using optical model potential (OMP) [7,8] and above 10 MeV by using JLM. We adjust the normalization constants for the OMP, because the agreement of the calculated cross sections with the data in very low incident energies of the neutron is insufficient without any adjustments. The energy dependent normalization constants, real part $\lambda_v$ and imaginary part $\lambda_w$, of the OMP and JLM are determined explicitly from the integrated elastic cross section data, respectively. Comparing the results of calculations with experimental data, we discuss that the present CDCC calculations, which reproduce the experimental data observed in incident energies higher than 10 MeV with the single folding potential of the JLM and in lower energies with introducing the normalization factors for the cluster folding potential of the OMP.

## 2 Method and Model

We prepare the wave functions of the bound and $\alpha$-*d,t* scattering states of $^{6,7}$Li in the similar way as previous work [1-3] in the CDCC method.

In $^6$Li case, the binding energy of the $1^+$ ground state is observed as 1.47 MeV with respect to the $^6$Li→ $\alpha$ + *d* threshold, and the low-energy part of the $\alpha$-*d* scattering phase shifts in the *S*-wave (*l*=0) and *D*-wave (*l*=2) have been obtained experimentally. The excited $3^+$, $2^+$ and $1^+$ states of $^6$Li are observed at 2.18, 4.31, and 5.68 MeV, respectively, which are considered to be the triplet resonance state in the $\alpha$-*d, D*-wave. According to the cluster model, the wave functions for the ground state ($1^+$) and the exited states are written as

$$\phi_{II}(^6Li;k) = A\left\{\varphi(\alpha)[\varphi_I(d)\otimes u_l(k,\ r)]_I\right\}, \tag{1}$$

where $\varphi(\alpha)$ and $\varphi_1(d)$ stand for the internal wave functions of the alpha and deuteron clusters, respectively.

The interaction between $\alpha$ and *d* has central and spin-orbit parts, which are parametrized by a two-range Gaussian form and by a two-range Gaussian-derivative form, respectively;

$$\begin{aligned} V^{CE}{}_l(r) &= \upsilon_{1,l}e^{-(r/r_{1,l})^2} + \upsilon_{2,l}e^{-(r/r_{2,l})^2} + V_{CL}(r) \\ V_l^{SO}(r) &= \upsilon_{1,l}^{SO}re^{-(r/r_{1,l})^2} + \upsilon_{2,l}^{SO}re^{-(r/r_{2,l})^2} \\ V_{CL}(r) &= \begin{cases} Z_1Z_2e^2/r, & r \geq R_{CL} \\ \left(Z_1Z_2e^2/(2R_{CL})\right)\left(3-r^2/R_{CL}{}^2\right), & r < R_{CL}. \end{cases} \end{aligned} \tag{2}$$

They are chosen *l* -dependently so as to reproduce well the energies of the ground and excited states and the $\alpha$-*d* scattering phase shifts. The parameter values are listed in Table 1.

**Table 1.** The parameters of the effective central and spin orbit potentials between $\alpha$ and *d* for $l$ = 0 and 2

| **Parameters** | $r_{1,l}$ (fm) | $r_{2,l}$ (fm) | $\upsilon_{1,l}$ (MeV) | $\upsilon_{2,l}$ (MeV) | $\upsilon_{1,l}^{(SO)}$ (MeV) | $\upsilon_{2,l}^{(SO)}$ (MeV) | $R_{CL}$ (fm) |
|---|---|---|---|---|---|---|---|
| $l$ = 0 | 2.191 | 1.607 | -105.85 | 46.22 | -- | -- | 3.00 |
| $l$ = 2 | 2.377 | 1.852 | -82.00 | 26.00 | -2.31 | 1.42 | 3.00 |

The Schrödinger equation of the $^6$Li + *n* scattering system, which is described by using the *n* + $\alpha$ + *d* three body model, is written as

$$\left[K_R + K_r + V_{d\alpha}(r) + U_{dn}(r_{dn}) + U_{\alpha n}(r_{\alpha n}) - E\right]\Psi_{JM}^{CDCC} = 0, \tag{3}$$

where *E* is the energy of the total system, vector ***r*** is the relative coordinate between α and *d,* ***R*** the one between the center of mass of the *d*- $\alpha$ pair and *n*, and $\boldsymbol{r}_{dn}(\boldsymbol{r}_{\alpha n})$ denotes the relative coordinate between two particles $d(\alpha)$ and *n*. Operators $K_r$ and $K_R$ are kinetic energies associated with ***r*** and ***R***, respectively, and $V_{d\alpha}(r)$ is the interaction between *d* and α. The total wave function $\Psi_{JM}$ with the total angular momentum *J* and its projection *M* on *z*-axis is expanded in terms of the orthonormal set of eigenstates $\phi_{II}$ of $H(^6\text{Li})$ for the $\alpha$-*d* system;

$$\begin{aligned} \Psi_{JM}^{CDCC} &= \sum_L Y_{JM}^{l_0I_0L}\phi_0(r)\hat{\chi}_{\gamma_0}(P_0,R)/R \\ &+ \sum_{i=1}^{N}\sum_{l=0}^{l_{\max}}\sum_I\sum_L Y_{JM}^{lIL}\hat{\phi}_{iII}(r)\hat{\chi}_{\gamma}\left(\hat{P}\ ,R\right)/R, \end{aligned} \tag{4}$$

where the spin and angular parts are described as

$$Y_{JM}^{lIL} = \left[[i^lY_l(\Omega_r)\otimes\eta_d]\otimes i^lY_L(\Omega_R)\right]_{JM}\varphi(\alpha)\varphi(d), \tag{5}$$

with

$$\hat{\chi}_{\gamma_0}(P_0,R) = \chi_{\gamma_0}(P_0/R), \quad \gamma_0 = (0,l_0,I_0,L,J) \tag{6}$$

$$\hat{\chi}_\gamma\left(\hat{P}_\gamma, R\right) = W_\gamma \chi_\gamma\left(\hat{P}_\gamma / R\right), \quad \gamma = (i, l, I, L, J)$$

On the right hand side of Eq.(4), the first term presents the elastic channel denoted by $\gamma_0$ and the second one corresponds to the discretized breakup channels, each denoted by $\gamma$. The expansion-coefficient $\chi_\gamma$ in Eq.(6) represents the relative motion between $n$ and $^6$Li, and $L$ is the orbital angular momentum regarding $\boldsymbol{R}$.

**Table 2.** Parameters of the optical potentials for $d$+$n$ and $\alpha$+$n$ at half the neutron incident energy.

| System | $V_0$(MeV) | $r_0$(fm) | $a_0$(fm) | $W_D$(MeV) | $r_{WD}$(fm) | $a_{WD}$(fm) |
|---|---|---|---|---|---|---|
| $d + n$ | 65.8 | 1.574 | 0.501 | 4.59 | 1.511 | 0.517 |
| $\alpha + n$ | 47.0 | 2.098 | 0.660 | 9.52 | 2.009 | 0.280 |

The interaction $U_{dn}$ ($U_{\alpha n}$) between $d$ ($\alpha$) and $n$ is taken to be the optical potential for $d$+$n$ ($\alpha$+$n$) scattering. In Table 2, the parameters are shown explicitly. For simplicity, the spin dependence of the interaction is neglected. In this study, we adopt $p$ + $\alpha$ scattering at 31MeV [7] instead of $n$-$\alpha$ interactions. For $n$ + $d$ scattering, we used a neutron potential parameter set presented by Wilmore et al. [8] at lower incident energies. However, these optical potentials cannot reproduce the calculated cross section of the $^6$Li + $n$ scattering. We introduce normalization parameters for real and imaginary parts of the cluster folding potential. We also use the JLM interaction based on a single folding model in the incident neutron energy region above 10 MeV. In the previous works [1-3], we reported the CDCC calculation with JLM interaction.

**Table 3.** The parameters of the effective central and spin orbit potentials between $\alpha$ and $t$ for $l$=1 and 3

| Parameters | $r_{1,l}$ (fm) | $r_{2,l}$ (fm) | $v_{1,l}$ (MeV) | $v_{2,l}$ (MeV) | $v_{1,l}^{(SO)}$ (MeV) | $v_{2,l}^{(SO)}$ (MeV) | $r_{1,l}^{(SO)}$ (fm) | $r_{2,l}^{(SO)}$ (fm) |
|---|---|---|---|---|---|---|---|---|
| $l$ = 1 ($3/2^-$) | 2.447 | -- | -84.70 | -- | -0.99 | -0.67 | 4.900 | 2.447 |
| $l$ = 1 ($1/2^-$) | 2.447 | -- | -89.50 | -- | -0.30 | -0.11 | 4.900 | 2.447 |
| $l$ = 3 | 2.608 | -- | -75.65 | -- | -1.05 | -- | 2.466 | 2.447 |

In $^7$Li case, we prepare the wave functions of the bound and $\alpha$-$t$ scattering states of $^7$Li in the similar way as the $^6$Li + $n$ reaction analysis in the CDCC method. The binding energy of the $3/2^-$ and $1/2^-$ bound states are observed as -2.47 MeV and -1.99 MeV, respectively, with respect to the $^7$Li→ $\alpha$ + $t$ threshold, and the low-energy part of the $\alpha$-$t$ scattering phase shifts in the $P$-wave ($l$ =1) and $F$-wave ($l$ = 3) have been obtained experimentally. The excited $7/2^-$ and $5/2^-$ states of $^7$Li are observed at 4.65 MeV and 6.60 MeV, which are considered to be the triplet resonance state in the $\alpha$-$t$ relative motion with the $F$-wave.

The potential between $\alpha$ and $t$ clusters is chosen $l$-dependently so as to reproduce well the energies of the ground state, and the excited states, and the $\alpha$-$t$ scattering phase shifts. The parameters are listed in Table 3.

**Table 4.** Parameters of the optical potentials for $t$+$n$ and $\alpha$+$n$ at half the neutron incident energy.

| System | $V_0$(MeV) | $r_0$(fm) | $a_0$(fm) | $W_D$(MeV) | $r_{WD}$(fm) | $a_{WD}$(fm) |
|---|---|---|---|---|---|---|
| $t + n$ | 50.35 | 2.146 | 0.144 | 0.520 | 2.164 | 0.378 |
| $\alpha + n$ | 47.00 | 2.098 | 0.660 | 9.520 | 2.009 | 0.280 |

The interaction $U_{tn}$ ($U_{\alpha n}$) between $t$($\alpha$) and $n$ is taken to be the optical potential for the $t$+$n$ ($\alpha$+$n$) scattering (Table 4). For simplicity, the spin dependence of the interaction is neglected. In this study, we adopt $p$ + $\alpha$ scattering at 31 MeV [7] instead of $n$-$\alpha$ interactions. For $n$ + $t$ scattering, we used a neutron potential parameter set presented by Wilmore et al. [8] at lower incident energies. However, these optical potentials cannot reproduce the experimental cross sections. Therefore, we introduce normalization parameters for real and imaginary parts. We also use the JLM interaction based on a single folding model in the incident neutron energy region above 14.1 MeV.

## 3 Result and discussion for $^{6}$Li

In this calculation, we analyze the integrated elastic and inelastic scattering cross sections of the $^{6}$Li+*n* collision at incident neutron energies below 10 MeV by using optical model potential (OMP) and above 10 MeV by using JLM for the $^{6}$Li-*n* folding potential. For the JLM single-folding potential, we take the normalization factors $\lambda_v$=1.0 and $\lambda_w$ =0.2 for the real and imaginary parts, respectively. These values indicate that the small imaginary potential is needed while the real part has no any adjustment parameter. This is consistent with the previous studies [1-3]. However, because the JLM potential has not been constructed for incident neutron energies lower than about 10 MeV [5], we cannot use the JLM single-folding potential for these energies. Instead of the microscopic JLM single-folding potential, we employ a more phenomenological cluster folding potential in lower energies.

We determine normalization factors, real part $\lambda_v$ and imaginary part $\lambda_w$, of the cluster folding $^{6}$Li-*n* potential using *α*-*n* and *d*-*n* OMPs from measured integrated elastic cross section data. The obtained factors are expressed as the following linearly energy dependent form:

$$\lambda_V(E) = 1.6 - 0.12E_n$$
$$\lambda_w(E) = 0 \quad (7)$$

Figure 1 shows the differential cross sections of the $^{6}$Li + *n* elastic scattering with incident energies between 1.5 and 24.0 MeV. One can see that the results of the CDCC calculation represented with solid lines are in good agreement with the experimental data.

For inelastic scattering, Fig.1 shows the angular distributions to the $3^+$ resonance state of $^{6}$Li for $E_n$=5.98, 7.5, 8.17, 10.27, 14.1, 18.0 and 24.0 MeV. The calculated differential cross sections are obtained by integrating the breakup cross section to several discretized $3^+$ solutions obtained around the resonance energy region. We can see that the CDCC calculation can also reproduce the inelastic observed cross sections together with the elastic ones.

We also calculate the integrated elastic and inelastic cross sections between 1.5 and 24.0 MeV. The integrated elastic cross sections for $^{6}$Li agree with the evaluated data (JENDL-3.3) and other measurements within the experimental uncertainties, as shown in Fig. 2. In Fig.3, the integrated inelastic cross-section values for the 2.186 MeV state of $^{6}$Li are almost in good agreement with the evaluation data of JENDL-3.3 and the experimental data.

## 4 Result and discussion for $^{7}$Li

In this calculation, we analyze the integrated elastic and inelastic scattering cross sections of the $^{7}$Li+*n* collision at incident neutron energies below 14.1 MeV by using the optical model potential (OMP) and above 14.1 MeV by using the JLM $^{7}$Li-*n* folding potential. For the JLM single-folding potential, we take the normalization factors $\lambda_v$ = 1.0 and $\lambda_w$ = 0.2 for the real and imaginary parts, respectively. These values of the normalization factors indicate that the small imaginary potential is needed while the real part has no any adjustment parameter.

We determine normalization factors, real part $\lambda_v$ and imaginary part $\lambda_w$, of the cluster folding $^{7}$Li-*n* potential using *α*-*n* and *t*-*n* OMPs from the integrated elastic cross section data. For the OMP cluster-folding potential, we assume $\lambda_w$ = 0 for all incident neutron energies lower than 14.1 MeV. The normalization factor $\lambda_v$ is determined at each incident energy below 5 MeV and introduced a linear energy-dependent form from 5 MeV to 14.1MeV. The obtained results of $\lambda_v$ are presented in Table 5.

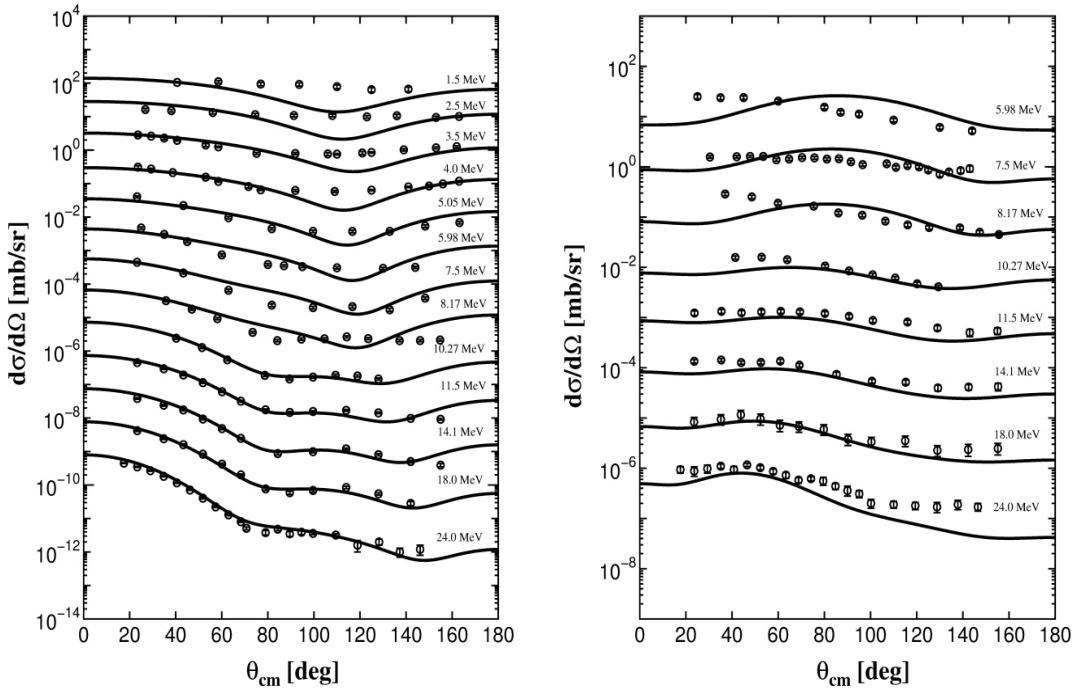


**Figure 1.** Elastic and inelastic angular distribution of the differential cross sections for the $^{6}$Li + *n* scattering for incident energies between 1.5 and 24.0 MeV. The solid lines and open circles correspond to the calculated data and experimental data. The data are subsequently shifted downward by a factor 1/10.

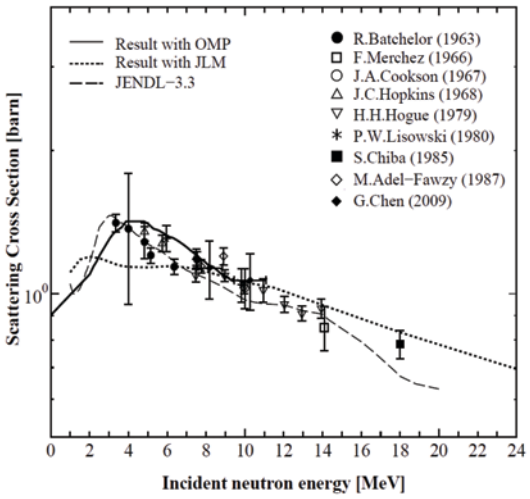


**Figure 2**. The integrated elastic scattering cross sections of $^{6}$Li, in comparison with the evaluated data and experimental data.

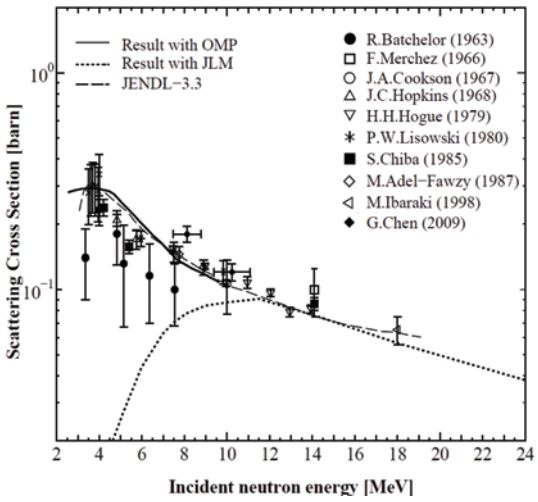


**Figure 3.** The integrated inelastic scattering cross sections for the $3^{+}$ state of $^{6}$Li, in comparison with the evaluated data and experimental data.

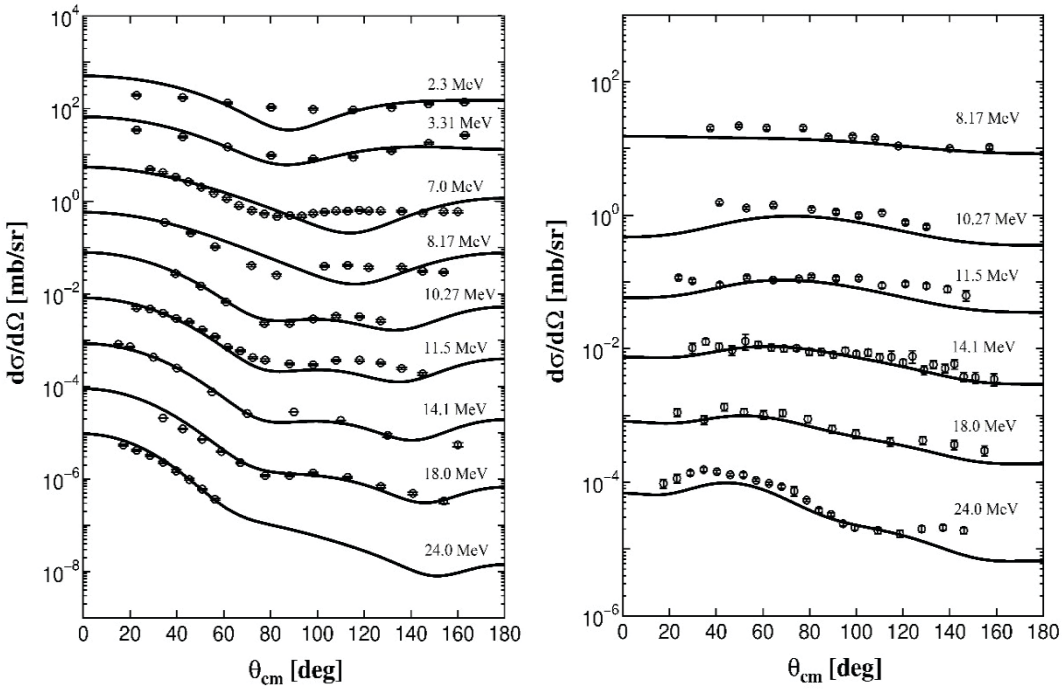


**Figure 4.** Elastic and inelastic angular distribution of the differential cross sections for the $^{7}$Li + *n* scattering for incident energies between 2.3 and 24.0 MeV. The solid lines and open circles correspond to the calculated data and experimental data. The data are subsequently shifted downward by a factor 1/10.

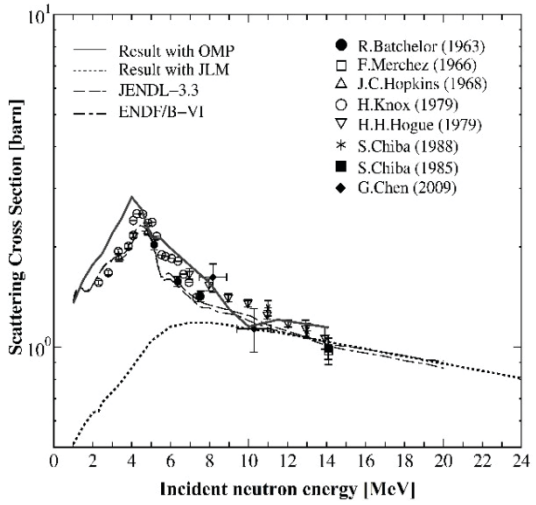


**Figure 5.** The integrated elastic scattering cross sections of $^{7}$Li, in comparison with the evaluated data and experimental data.

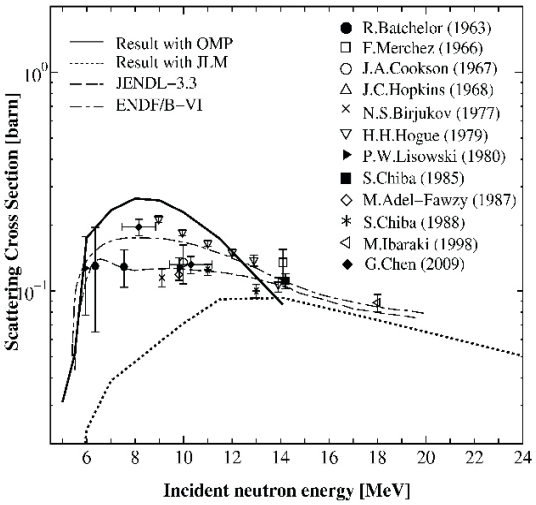


**Figure 6.** The integrated inelastic scattering cross sections for the 4.65 MeV state of $^{7}$Li, in comparison with the evaluated data and experimental data.

Table 5. The normalization factors $\lambda_v$

| Neutron energy $E_n$ (MeV) | Normalization factors $\lambda_v(E_n)$ |
|---|---|
| 1.0 | 0.760 |
| 1.5 | 0.740 |
| 2.0 | 1.050 |
| 2.5 | 1.117 |
| 3.0 | 1.220 |
| 3.5 | 1.400 |
| 4.0 | 1.360 |
| 4.5 | 1.340 |
| 5.0 | 1.000 |
| $5.5 \leq E_n \leq 14.1$ | $1.7–0.07E_n$ |

The left hand panel of Fig. 4 shows the differential cross sections of the $^7$Li + *n* elastic scattering with incident energies between 2.3 and 24.0 MeV. One can see that the results of the CDCC calculation represented with solid lines are in good agreement with the experimental data. The angular distributions show rather flat in low energy cases in comparison with high energy ones. It seems to be due to increase of the *s*-wave contribution. For inelastic scattering, the right hand panel of Fig.4 also shows the angular distributions to the $7/2^-$ resonance state of $^7$Li for $E_n$ = 8.17, 10.27, 11.5, 14.1, 18.0 and 24.0 MeV. The calculated differential cross sections are obtained by integrating the breakup cross section to several discretized $7/2^-$ solutions obtained around the resonance energy region. We can see that the CDCC calculation can also reproduce the inelastic observed cross sections together with the elastic ones.

We also calculate the integrated elastic and inelastic cross sections between 1.0 and 24.0 MeV. The integrated elastic cross sections for $^7$Li almost agree with the evaluated data (JENDL-3.3 and ENDF/B-VI) and other measurements within the experimental uncertainties, as shown in Fig. 5. In Fig.6, the integrated inelastic cross-section values for the 4.65 MeV state of $^7$Li are almost in good agreement with the evaluation data and the experimental data.

## 5 Summary

Applying the CDCC framework to the $^6$Li ($\alpha$-*d*)+*n* and $^7$Li ($\alpha$-*t*)+*n* models, we investigated the integrated neutron elastic and inelastic scattering cross sections for the $^6$Li and $^7$Li targets, respectively, at incident neutron energies below 10 MeV using the cluster-folding of the optical model potentials and above 10 MeV using the JLM single-folding potential. Energy dependence of the normalization factors, $\lambda_v$ and $\lambda_w$, of the cluster folding potential is introduced and determined from measured integrated elastic cross sections. The CDCC calculation gives a satisfactorily good agreement with the experimental data.

Although our model calculation is still difficult to reproduce low energy data below 14.1 MeV without adjusting nomarlization factor. This may suggest limitation of applying our model. Therefore it is desirable to extend the CDCC method with other reactions processes such as compound reaction.

## Acknowledgements

This work was supported by Japan Society for Promotion of Science (JSPS) for "'R&D' Platform Formation of Nuclear Reaction Data in Asian Countries (2010-2013)", Asia-Africa Science Platform Program and Grant-in-Aid for Publication of Scientific Research Results (No. 257005). Furthermore, this work was supported by Ministry of Education and Science of Republic Kazakhstan for Promotion of Science (the grant No. 3106/GF4).

## References

1. T. Matsumoto, D.Ichinkhorloo, Y.Hirabayashi, K.Katō, and S.Chiba, Phys. Rev. C **83**, 064611, (2011)

2. D.Ichinkhorloo, T.Matsumoto, Y.Hirabayashi, K.Katō and S.Chiba, J. Nucl. Sci. Technol. Vol.**48**, No. 11, pp. 1357-1460 , Sep. 2011
3. D.Ichinkhorloo, Y.Hirabayashi, K.Katō, M. Aikawa, T.Matsumoto, and S.Chiba, Phys. Rev. C **83**, 064604, (2012)
4. M.Kamimura, M.Yahiro, Y.Iseri, Y.Sakuragi, H.Kameyama and M.Kawai, Prog. Theor. Phys. Suppl. No. 89 (1986),
5. J.-P. Jeukenne, A. Lejeune, and C. Mahaux, Phys. Rev. C **16**, 80 (1977).
6. H.Guo, Y.Watanabe, T.Matsumoto, K.Ogata and M.Yahir, Phys. Rev. C **87**, 024610 (2013).
7. S. J. Burger and G. Heymann, Nucl. Phys. A **243**, 461 (1975)
8. D.Wilmore and P.E.Hodgson ,Nucl. Phys. 55, 673 (1964)
9. G.Chen, X.Ruan, Z.Zhou, J.Zhang, B.Qi, X.Li, H.Huang, H.Tang, Q.Zhong, J.Jiang, B.Xin, J.Bao, and L.Chen, Nuclear Science and Engineering **163**, 272–284 (2009)
10. A.B.Smith et al, J,NP/A,373,305,8201 (1982)
11. H.H.Hogue et al., J. Nucl. Sci. Eng., **69**, 22 (1979)
12. P.W.Lisowski et al., LA-8342, Los Alamos Scientific Laboratory (1980)
13. J.A.Cookson et al., J. Nucl. Phys. A, **91**, 273 (1967)
14. M.Adel-Fawzy et al., Nucl. Instrum. Methods, **169**, 533 (1980)
15. R.Batchelor et al., J. Nucl. Phys., **47**, 385 (1963)
16. J.C.Hopkins et al., J. Nucl. Phys. A, **107**, 139 (1968)
17. F.Merchez et al., J. Physique Colloque, **27**, 1, 61 (1966)
18. S.Chiba al., J. Nucl. Sci. Technol., **25**, 2, 210 (1985)
19. M.Ibaraki et al., JAERI-Research 98-032, Japan Atomic Energy Research Institute (1998)